JOURNAL OF MATERIALS SCIENCE **40** (2005) 6399–6407

The growth and electrical transport properties of self-organized metal/oxide nanostructures formed by anodizing Ta-Al thin-film bilayers

A. MOZALEV, G. GOROKH
Department of Microelectronics, Belarusian State University of Informatics and Radioelectronics, Brovka Str. 6, Minsk 220013, Belarus

M. SAKAIRI, H. TAKAHASHI
Laboratory of Interface Micro-Structure Analysis, Graduate School of Engineering, Hokkaido University, N-13, W-8, Kita-ku, Sapporo 060-8628, Japan

Published online: 5 October 2005

Anodizing of Ta-Al metal bilayers (Al on Ta) sputter-deposited onto SiO_2 substrates was performed in oxalic acid electrolytes at anode potentials of 53 to 21.5 V in order to form nanoporous alumina layers and sequentially oxidize the tantalum underlayers through the alumina pores. The films formed consist of arrays of tantalum oxide nanohillocks percolating through the residual tantalum layer down to the substrate, so that a self-organized network of tantalum nanowires forms between the substrate and the alumina film. The average width (25–<10 nm), length (70–35 nm), and population density (10^9–10^{11} cm^{-2}) of the nanowires are systematically defined by the initial tantalum thickness (8–22 nm) and the anodizing conditions. The mesh-like, nano-sized morphologies of the tantalum underlayers result in a remarkably wide range of potential-dependent, controlled electrical sheet resistances (10^2–10^7 Ω/sq). The periodical, tunable, metal/insulator film structure, allowing an increased transition to hopping or tunneling conduction at elevated temperature, leads to negative temperature coefficients of resistance, ranging 300 to 5 ppm/K. Oscillations of the potential-dependent dc conductance registered in the films at room temperature are attributed to the quantum-size effects in the metal/oxide nanostructures. The films are of technological importance for fabrication of thin-film, planar, adjustable resistors with significantly improved performances.

1. Introduction

The development of advanced systems and materials components at the nanoscale whose structures exhibit unusual physical and chemical properties will be a future challenge in materials science and engineering industry [1]. Ideally, these systems should show significantly improved performance in some sense. Recent studies have shown that anodizing under certain conditions of sputter-deposited Ta-Al, Nb-Al, and Ti-Al metal bilayers (tantalum, niobium, or titanium layer covered with a thin aluminum layer) results in the formation of self-organized arrays of nanostructured anodic oxides, of unique morphologies, complex chemical compositions, and diverse physical and functional properties [2, 3]. Although for years there has been the interest to these nanostructured anodic oxides, the residual (unanodized) valve-metal layers, remaining underneath the porous alumina films, have received limited study. For example, one of the present authors has found that the underlying tantalum film of a certain thickness can be consumed locally down to the substrate by anodizing the Ta-Al bilayer in 0.6 M citric acid electrolyte [4]. This results in the formation of a mesh-like tantalum film of significantly increased electrical resistivity. However, after completing the formation process, the porous alumina layer was supposed to be selectively dissolved and not to be used along with the residual tantalum underlayer. This has been major limitation of the technology for fabricating thin-film resistors incorporated in the planar, multilayered structures because the removal of the porous alumina layer results in the formation of unacceptable gaps around the resistors and aluminum lines, and this destroys the planarity of the interconnection level [5–8]. Moreover, as the films described in early work [4] were formed at a high anodic voltage of 250 V, the average sizes of the tantala bulges and the metallic intervals between them (typically 500–150 nm) were not yet quantum-sized to expect the existence of pronounced confinement-enhanced effects in the electron transport in the films.

0022-2461
DOI: 10.1007/s10853-005-1620-9

In this paper, we have employed oxalic acid electrolytes, giving low formation potentials, for anodic oxidation of Ta-Al metal bilayers sputter-deposited onto dielectric substrates, striving to achieve the formation of metal/oxide nanostructures of sizes systematically varied from 90 to <10 nm, i.e. by one order of magnitude smaller than those described in early work [4]. The thickness range for the tantalum underlayers has been selected to allow their local oxidation down to the substrate, so that to prepare mesh-like tantalum films, clad with the porous alumina layers, and expect an unconventional electrical behavior of the films, due to their unique self-organization at the nanoscale. The morphologies and chemical compositions of the anodically formed films have been investigated by scanning (SEM) and transmission electron microscopy (TEM), X-ray photoelectron spectroscopy (XPS) depth profiling, and energy-dispersive X-ray (EDX) point analysis. Dielectric properties of the nanostructured anodic oxides have been examined by electrochemical impedance spectroscopy (EIS). Electrical transport phenomena in the residual tantalum films, sandwiched between the dielectric substrate and the alumina layers, have been studied by dc measurements in a temperature range.

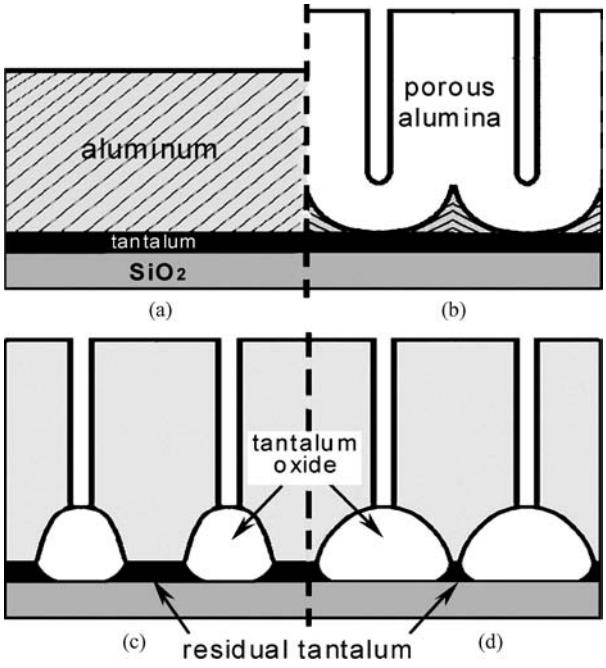

Figure 1 Schematic diagram showing the main steps to form nanostructured metal/oxide films: (a) sputter-deposition of a Ta-Al bilayer, (b) formation of a porous anodic film from the overlying Al in a solution of oxalic acid, (c) anodizing of the Ta underlayer, (d) reanodizing of the Ta underlayer to a higher potential.

2. Experimental

2.1. Specimen preparation

Thin tantalum layers, of 8 to 22 nm thickness, followed by aluminum layers, 500 nm thick, were sputter-deposited by a dc magnetron method onto oxidized silicon wafers to form the Ta-Al bilayer samples. Similarly, the Ta-Al bilayers were deposited onto oxide-coated aluminum foils that provide flat surfaces and are appropriate for later TEM. The silicon and aluminum substrates were then cut into of 2 cm × 2 cm pieces and anodized in a specially designed three-electrode cylindrical cell with an aluminum counter electrode and a PTFE protecting ring defining a working area within a circle of 1.5 cm^2. The reference electrode was an Ag/AgCl electrode connected to the working solution by a capillary containing agar-agar and KCl.

The main steps to form the metal/oxide films from the sputter-deposited Ta-Al bilayer are shown schematically in the diagram of Fig. 1. Firstly, the overlying aluminum was anodized to form porous anodic film (Fig. 1a and b). This anodizing was performed in stirred oxalic acid solutions of various concentrations in the range 0.9–0.05 M at constant anode potentials E_a of 21.5 to 53 V. After the aluminum layer was fully consumed, anodizing was sequentially continued at the same value of anode potential until the current lowered to its leakage value, of about 3 μA cm^{-2}. During the current-decay period, oxidation of the underlying tantalum occurred under the bottoms of the alumina cells, and an array of nano-sized tantala hillocks, incorporated in the depth of the tantalum layer and reaching the substrate, was expected to form due to self-organization at the tantalum/alumina interface (Fig. 1c). Following anodizing, some of the specimens were reanodized [2, 9] in stirred 0.1 M citric acid solution by sweeping anode potential at a constant rate of 50 mV s^{-1} to a higher value (hereafter referred to as the reanodizing potential E_R) starting from that used at the fist anodizing stage for each specimen. This was expected to further consume the remaining tantalum metal, locally and underneath the alumina pores, proportionally to E_R value, as suggested schematically in Fig. 1d.

2.2. Film characterization

Surfaces and cross-fractures of the anodized Ta-Al bilayers onto the silicon wafers were observed using a Hitachi S-806 scanning electron microscope operated at 20 kV. Before observations, a gold layer, less than 3 nm thick, was evaporated onto the fractures and surfaces of all specimens. A hot mixture of phosphoric and chromic acid solutions (designated "selective etchant") prepared in the usual way [10] was used in this work for dissolving the porous alumina films before SEM observations. Ultramicrotomed sections of the anodized bilayers formed onto the oxide-coated aluminum foils were prepared using a Reichert-Nissei Ultracuts/FCS ultramicrotome, following the procedure described elsewhere [11]. Ultramicrotomed sections, collected onto copper grids, were examined in a Hitachi H-700H transmission electron microscope operated at 200 kV. Elemental analysis by EDX was performed in a JEOL JEM-2000ES electron microscope, and an electron probe, of diameter about 15 nm, was employed to optimize spatial resolution and X-ray count rates. XPS depth profiling analysis was carried out in a VG Scientific ESCALAB Mk II triple channeltron analyzer with Al Kα-ray excitation; the details of the procedure were the same as described in previous work [3]. Impedance measurements of specimens formed at different anode potentials were carried out in 0.5 M H_3BO_3/0.05 M $Na_2B_4O_7$ solution (pH 7.4) at 296 K with an FRA 5095 frequency response analyzer (NF Corp.). The applied

sinusoidal signal amplitude was 100 mV over the frequency range of 1 MHz–2 MHz. The computer system integrated in this device was used for measurement and data storage. The measured data were analyzed by a computer simulation and fitting program. Details of the procedure have been described elsewhere [12].

3. Results

3.1. Microscopic observations

SEM images of the nano-sized tantala hillocks derived from the Ta(8 nm)-Al bilayers, anodized at various anode potentials, are presented in Fig. 2 (the overlying porous alumina had been removed in the selective etchant). From the SEM observations, the population density of the hillocks coincides with that of pores in the corresponding alumina film, which implies that the hillocks grow right underneath the alumina cell. From the surface views of Fig. 2, the hillocks are shaped as distorted hexagons with wide bases and rather smooth edges. An important feature to be considered is that the intervals between the hillocks (black areas in the micrographs), presumably unanodized tantalum metal, are self-organized in a regular network of tantalum nanowires (for definition of the meaning of "nanowires" see the sketch drawn over the micrograph of Fig. 2c. From the surface views of Fig. 2, the nanowires thin and narrow with reducing the formation potential. Importantly, no residual aluminum metal is observed over the tantalum surface at the available resolution. The width of the nanowires remains rather constant over the whole surface or each specimen.

Fig. 3a shows a SEM image of a cross-fracture of the Ta(22 nm)-Al bilayer prepared onto the oxidized silicon wafer and anodized at 53 V. Fig. 3b displays a TEM image of an ultramicrotomed cross-section of the similarly anodized bilayer prepared onto the oxide-coated

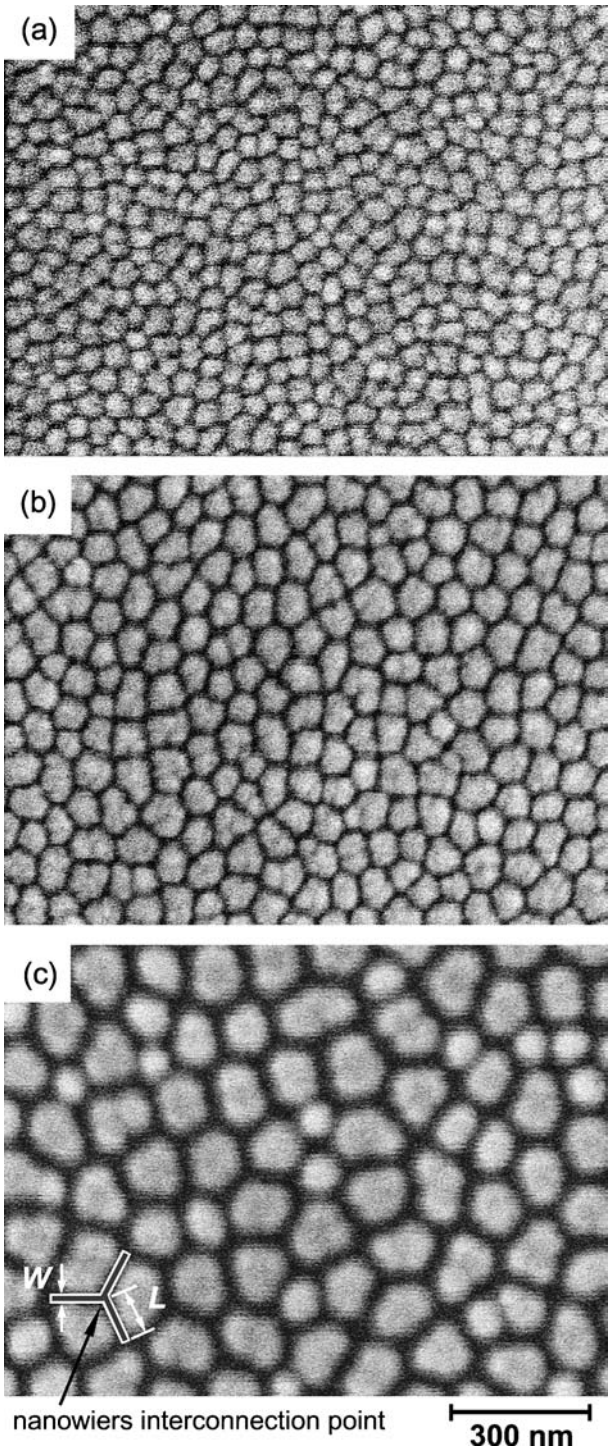

Figure 2 SEM surface views of the metal/oxide nanostructures derived from the Ta(8 nm)-Al bilayers anodized (a) at 21.5 V in 1.0 M $H_2C_2O_4$ at 308 K, (b) at 30 V in 0.9 M $H_2C_2O_4$ at 303 K, and (c) at 53 V in 0.2 M $H_2C_2O_4$ at 293 K. The overlying anodic alumina had been dissolved in 20 g/l CrO_3/35 ml/l H_3PO_4 at 343 K.

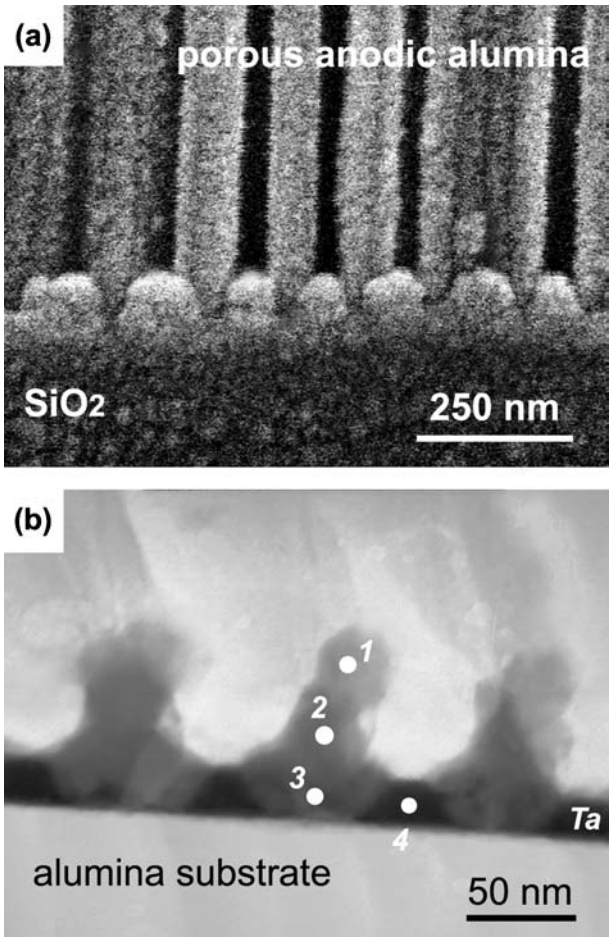

Figure 3 (a) SEM image of a cross-fracture of the anodized Ta(22 nm)-Al bilayer prepared onto an oxidized silicon wafer, (b) TEM image of a cross-section of the anodized Ta(22 nm)-Al bilayer prepared onto an oxide-coated aluminum substrate. In both cases anodizing was done in 0.2 M $H_2C_2O_4$ at 53 V.

TABLE I Geometrical parameters of the tantalum nanowires derived from the Ta(8 nm)-Al bilayer anodized at various anode potentials (without reanodizing)

Anode potential E_a (V)	Population density N_w (cm^{-2})	Average length L (nm)	Average width W (nm)
53.0	2.1×10^9	70	25
30.0	5.8×10^{10}	50	15
21.5	1.3×10^{11}	35	10

aluminum substrate. From the TEM view, the tantalum metal is consumed locally down to the substrate, so that the tantalum oxide hillocks percolate through the residual tantalum layer, thus defining the mesh-like structure of the residual tantalum layer. Examination of many specimens formed at various anodizing conditions confirmed that the nanohillocks and nanowires all became smaller with decreasing E_a. For the specimens formed at the same anode potentials, the tantalum wires narrowed while the oxide hillocks expanded along the substrate with decreasing d. Further, the population density of the hillocks N_h and that of the nanowires N_w both increased with lowering E_a, although did not change with d decreasing. The selected numerical results obtained for the anodized Ta(8 nm)-Al bilayer are presented in Table I.

3.2. XPS and EDX analysis

The Ta(22 nm)-Al bilayer anodized in 0.2 M $H_2C_2O_4$ electrolyte at 53 V was chosen as a model system for XPS analysis. Before XPS experiments, the overlying alumina had been removed in the selective etchant; the surface of the specimen was as shown in Fig. 2c. Depth profiling was performed for tantalum, oxygen, and carbon identified in the XP survey spectrum and represented by Ta 4f, O 1s, and C 1s peaks. C1s at 285 eV was used as the reference binding energy for all spectra collected. The measured carbon peak weakened sharply after the first Ar^+ sputtering cycle (every sputtering cycle lasted 1 min) and became negligible beyond 3 min sputtering. This indicates that the carbon peak originated from contaminant hydrocarbon absorbents but not from carbon-containing species incorporated in the anodic film.

The selected XPS Ta4f peaks as a function of sputtering time are shown in Fig. 4. The spectrum of the unsputtered surface consists of two doublet peaks ($4f_{7/2}$ and $4f_{5/2}$), corresponding to the Ta^{5+} state at 26.4 and 28.2 eV and to the Ta^0 state at 21.2 and 23.0 eV. The intensities of both peaks rise after the first sputtering cycle. With further sputtering, the intensity of the Ta^{5+} doublet scarcely changes while the intensity of the Ta^0 doublet continues to increase until the two peaks become rather comparable. After about 14 min sputtering, the intensities of the Ta^{5+} and Ta^0 peaks decrease sharply and both peaks soon vanish from the spectrum. Obviously, the presence of metallic tantalum peak already at the film surface and its increasing intensity throughout the film depth is consistent with the tantalum metal intervals between the hillocks, which widen along the substrate surface due to the trapezoidal profile

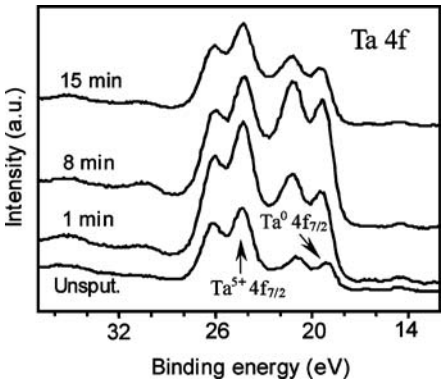

Figure 4 XPS Ta 4f peaks as a function of Ar^+ sputtering time for the metal/oxide film derived from the Ta(22 nm)-Al bilayer anodized in 0.2 M $H_2C_2O_4$ at 53 V (the overlying alumina had been dissolved as in Fig. 2).

of the hillock bottoms incorporated into the tantalum layer, as seen in Fig. 3b.

The measured spectrum of O 1s for the one-minute sputtered surface consisted of a symmetrical peak at 530.5 eV (not shown here) that is assigned to oxygen bound in tantala. With further sputtering, the intensity of the O 1s peak decreased monotonously until oxygen bound in silicon dioxide in the substrate began to influence the O 1s spectra.

The evolution of the Ta 4f peaks, complemented by the O 1s peak profiling behavior and supported by the results described in Ref. [2, 3, 13], suggests that there exists in the hillock depth oxidized tantalum in its lower than +5 state.

For the same specimen, the presence of tantalum suboxides in the hillock depth was further confirmed by EDX point analysis of the ultramicrotomed sections at the positions marked approximately on the micrograph of Fig. 3b. Table II shows the average atomic ratio of oxygen to tantalum in the Ta-O system at the marked positions. From the Table II, the atomic ratio in the upper part of the selected hillock corresponds to the stoichiometric tantalum pentoxide (2.5), but than lowers to 2.0 in the middle part of the hillock, decreasing eventually to 0.95 in the hillock base. The value of 0.15 for the atomic ratio registered within the residual tantalum underlayer [point 4 in Fig. 3b] appeared to be equal to that determined for the as deposited tantalum film. This indicates that the residual (unanodized) tantalum was completely excluded from the ionic-current passway and thus was not oxidized during the formation process. The main revelation from the XPS and EDX results is that, in the in-plain direction, the metal nanowires and their interconnection points are all surrounded by oxygen-deficient tantalum monoxide.

TABLE II Results of EDX point analysis of the anodized Ta (22 nm)-Al bilayer at probe positions marked on TEM photograph of Fig. 3b

Beam position	[O]/[Ta] (at. ratio)
1	2.5
2	2.0
3	0.95
4	0.15

3.3. Electro-physical properties

3.3.1. EIS measurements

The electro-conducting behavior of the anodized Ta-Al bilayer in the direction normal to the substrate was examined by EIS. Fig. 5 shows, as a typical example, the measured impedance bode diagrams for the film grown at 53 V from the Ta-Al bilayer with a 'non-limited-thickness' tantalum underlayer. It is seen that, in logarithmic axes, the impedance value vs. frequency curve can be divided into three characteristic parts: a horizontal straight line in the low-frequency range, a straight line with a slope of –1 in the middle-frequency range and a horizontal straight line in the high-frequency region. The phase shift changes from 0° through almost –90° to 0° with frequency increasing. The bode diagrams suggest a simple equivalent circuit for the films, as inserted in Fig. 5a. In the circuit, C is the parallel capacitance of the film, R_f is the parallel resistance of the film, and R_{sol} is the resistance of the solution. A fit of the impedance data for the circuit of Fig. 5 was in very good agreement with the experimental data.

For the films formed at 21.5 and 30 V, the bode diagrams (not shown here for simplicity) were similar to the diagrams of the specimen formed at 53 V. This implies the same equivalent circuit for each specimen as inserted in Fig. 5a and its similar interpretation. With increasing E_a, the straight line of the Z-F curve in the middle-frequency region and the phase-shift-frequency curve moved to the higher frequency direction. This may only resulted from a change in the capacitance value in the equivalent circuit.

3.3.2. Measurements of dc conductance

For measuring the in-plain conductivity (i.e. along the substrate surface) of the nanostructured metal/oxide films, test resistors were prepared as follows. Pairs of parallel tantalum protecting masks, at a distance of 3 μm, reaching the dimensions of macroscopic end contacts, were formed over the aluminum film in the Ta-Al bilayers by means of sputter-deposition, photolithography, and chemical etching, generally following the procedure described in Ref. [5, 14]. Then the samples were anodised as described in Section 2.1. The area defined for anodizing was a 3 × 30 μm quadrangle (0.1 square). Fig. 6 shows a schematic view and a SEM image of a cross-section of the test resistor prepared and employed in this study. Resistance of the test resistors was measured with a digital ohmmeter while the sheet resistance in ohm per square, R_S, was calculated using the following equation [18]:

$$R_S = RL^{-1}W, \tag{1}$$

where W is the resistor width; L is the resistor length, and R is the resistance value. Considering $L = 3$ μm and $W = 30$ μm, Equation 1 becomes

$$R_S = 10R \tag{2}$$

Temperature coefficients of resistance (TCR's) were determined from the measured resistance values in the temperature range 283–393 K, as described elsewhere [18].

Electrical properties of the metal/oxide films were assessed by considering the changes in R_S (hereafter referred to as the resistance) with respect to d, E_a, and E_R. Variations of R_S with d in the Ta-Al bilayers anodized at various E_a are shown in Fig. 7. From the figure, the resistance exhibits sharp rise, at a progressively increasing rate, with thinning the tantalum underlayer whereas the thickness-dependent R_S for the as deposited tantalum films only shows weak proportional growth. Moreover, the dynamic growth process influenced by reanodizing gives anomalous behavior of the potential-dependent resistance, displayed in Fig. 8. When the reanodizing potential is raised, the measured resistance increases, at an increasing rate, until a drop

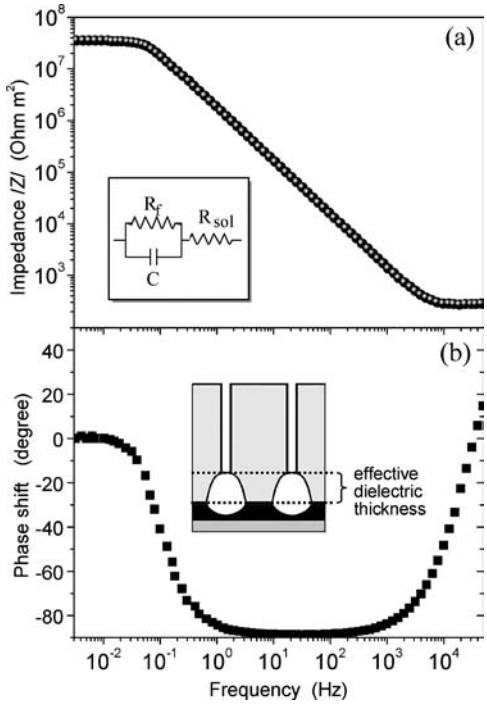

Figure 5 (a) Bode plot—modulus of impedance vs. frequency and (b) Bode plot—phase angle vs. frequency for the Ta(200 nm)-Al bilayer which had been anodized in 0.2 M $H_2C_2O_4$ at 53 V.

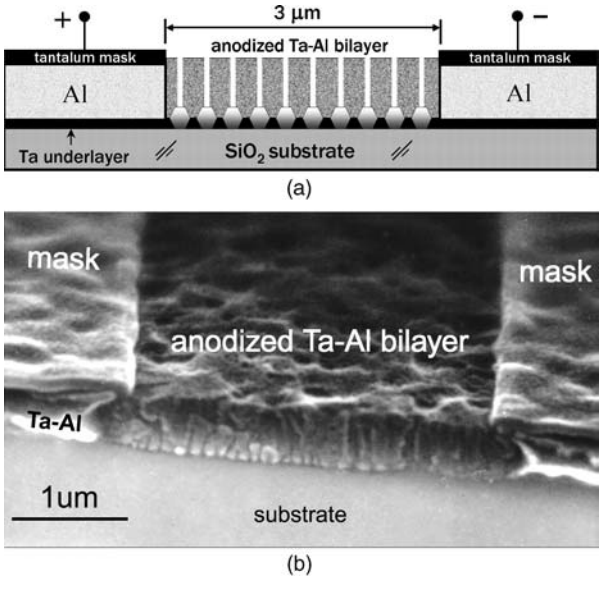

Figure 6 (a) Schematic cross-sectional view and (b) SEM image of a fracture of the test resistor prepared from the anodized Ta-Al bilayer.

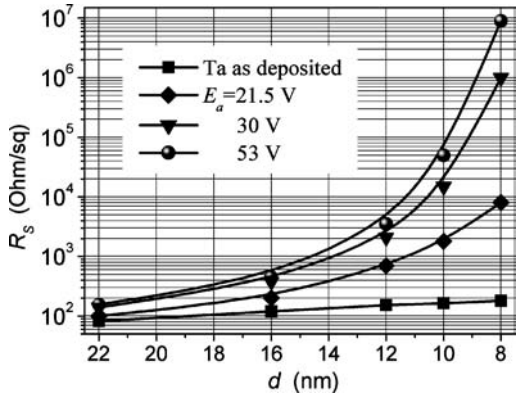

Figure 7 Variation of sheet resistance R_S with thickness of tantalum underlayer d in the Ta-Al bilayer anodized at various anode potentials E_a.

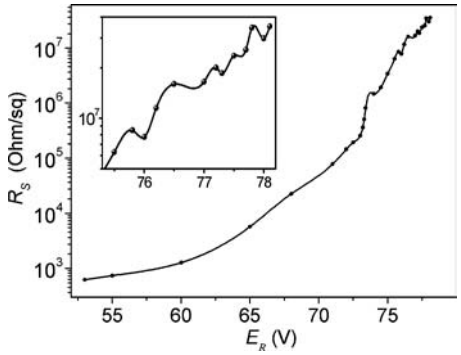

Figure 8 Room temperature dependence of sheet resistance R_S on reanodizing potential E_R for metal/oxide films derived from the Ta(16 nm)-Al bilayer initially anodized in 0.2 M $H_2C_2O_4$ at 53 V and then reanodized in 0.1 M citric acid.

in the resistance first appears at about 74 V. Further increment in E_R leads to an oscillatory behavior for the resistance: distinct minima and maxima appear in the high-voltage part of the R_S-E_R curve, until the resistance reaches an unmeasured value.

All the metal/oxide films prepared in this study were characterized by negative TCR's. The absolute TCR value decreased with increasing E_a and with reducing d, the tendency being shown in the graphs of Fig. 9. Reanodizing of the films to a higher voltage was found to further lower the temperature coefficients. Practically, the lowest TCR values, in the range 5–10 ppm/K, were achieved in the films initially formed at 53 V and then reanodized to above 60–65 V.

4. Discussion

4.1. The growth of the metal/oxide nanostructures

The model of nucleation and growth of nanostructured oxide hillocks during anodizing the Ta-Al bilayer with a non-thickness-limited tantalum has been discussed in detail in previous work [3]. Inheriting the assumptions of the work, the model of ionic transport processes is now justified for the Ta-Al bilayer with the thickness-limited tantalum. Schematic cross-section views showing the main steps of the formation process are illustrated in Fig. 10. When the barrier layer of growing porous alumina film is just commencing to touch the tantalum underlayer, tantalum oxide nuclei form at the

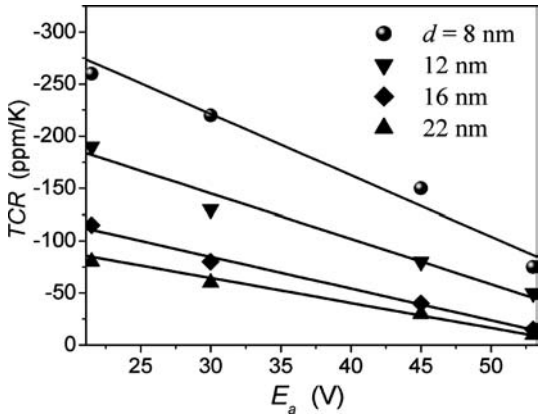

Figure 9 Variation of temperature coefficient of resistance (TCR) with anode potential E_a for the Ta-Al bilayers with different tantalum thicknesses d.

tantalum/alumina interface (Fig. 10a). Oxygen ions migrating inwards through the barrier layer are continuously injected into the growing tantala nuclei while the barrier layer is simultaneously eliminated at the tantala/alumina interface due to field-assisted dissociation of the Al–O bonds. The O^{2-} ions released from the dissociating alumina at the tantala/alumina interface are also injected into the growing hillocks while the released Al^{3+} ions migrate outwards through the remaining barrier layer and are expelled mostly in the electrolyte. The oxygen ions injected into the growing tantala hillocks then migrate inwards, and the tantalum layer is anodized to form oxide at the tantalum/tantala interface (Fig. 10b). However, the presence of tantalum suboxides in the hillock composition and their increasing content in the hillock depth suggest that the transport numbers for the Ta^{5+} and O^{2-} ions deviate from those commonly accepted for anodic films grown on uncovered tantalum layers in variety of electrolytes [15]. Further, owing to rather comparable ionic resistivities of tantalum oxide in the hillocks and aluminum oxide in the barrier layer, the adjacent aluminum metal is completely consumed during the current-decay period, and the pore bottoms partly dissolve and reshape (Fig. 10b). Due to the insufficient tantalum thickness for the hillocks to grow deeper, they spread in the direction along the film interface, consuming tantalum from the intervals between them. As a result, the hillocks grow somewhat smaller in height—the thinner the tantalum the lower the high. With increasing the reanodizing potential, the metallic intervals further narrow due to the increasing amount of consumed tantalum. This process continues until the electrical resistivity of the residual tantalum network becomes comparable to the ionic resistivity of anodic oxides in the complex film structure (Fig. 10c). Thus, for the oxalic acid electrolytes, the combination of d, E_a, and E_R. mainly defines the geometry of tantalum nanonetwork derived from the thickness-limited tantalum underlayers.

4.2. Dielectric properties of the nanostructured anodic oxides

The typical impedance diagrams shown in Fig. 5 demonstrate that the anodically formed films prepared

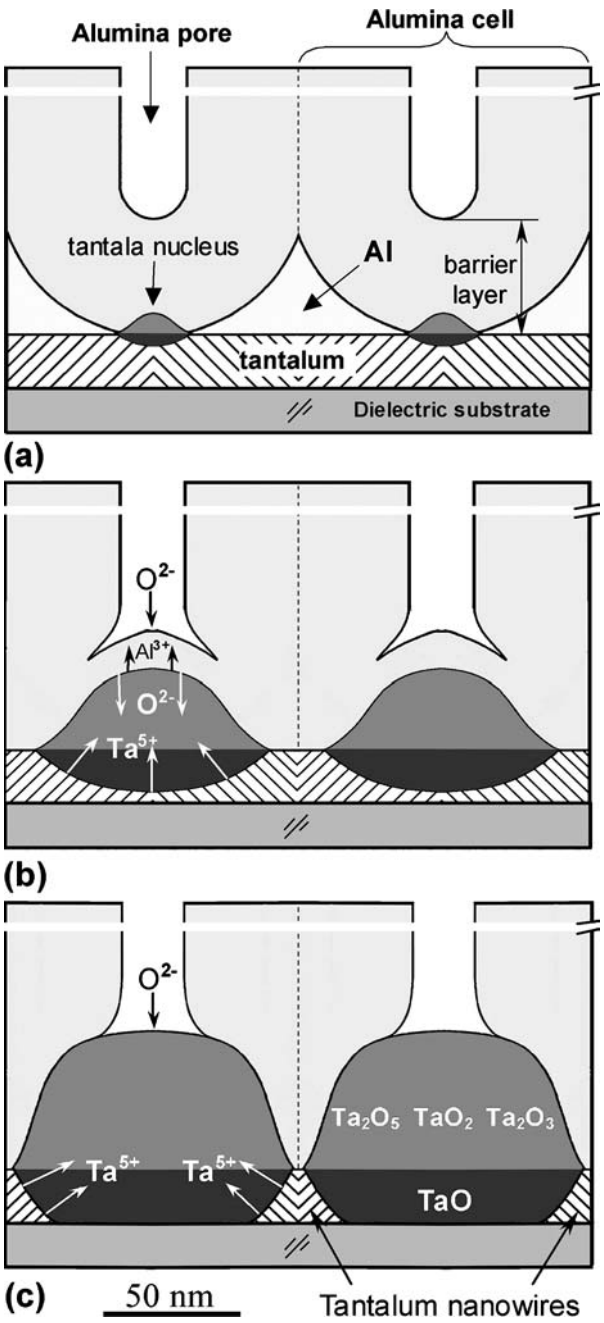

Figure 10 Schematic diagram showing the principle steps of modification of the tantalum/alumina interface and the general ionic transport processes during anodizing the Ta(22 nm)-Al bilayer (0.2 M $H_2C_2O_4$ at 53 V).

in this study behave as a nearly ideal stoichiometric oxide. From the measured bode plots, high values of R_f are obtained, representing the leakage resistance of the dielectrics. The magnitudes obtained are in good agreement with the electronic nature of the anodic films, which behave either as wide-band-gap semiconductors or insulators. The perfectly fitted bode diagrams for the tantalum/film/solution system can be explained through the following consideration. First, the parts of the alumina pores not occupied by the oxide hillocks are short-circuited by the solution filling the pores and covering the surface of the alumina film [16]. Similarly, the hillock bases are short-circuited by the residual tantalum metal, surrounding the hillock bases underneath the alumina film. This means that the nonstoichiometric tantalum monoxides, composing the hillock bases, do not worsen the dielectric behavior of the oxide hillocks in the direction normal to the film surface. Practically, the parallel capacitance determined from these experiments is that of tantalum/isolator/solution capacitor, in which the isolator is the exact combination of anodic alumina in the lower parts of the alumina cells and tantalum suboxides within the hillocks, as shown schematically in the insert of Fig. 5b. The dielectric behavior of this combination appears to be very close to that of an ideal capacitor.

The presence of mixed substoichiometric tantalum oxides in the hillock material results in the absence of electronically sharp interfaces, so that the dielectric lying between the tantalum substrate and the solution cannot be considered as a combination of several distinct dielectrics. This explains the simple equivalent circuit (see Fig. 5a) for the nanostructures prepared in this study.

4.3. Transport properties of the tantalum nanowires

Apparently, the significantly enlarged values of electrical resistivities for the anodized Ta-Al bilayers (see Fig. 7) arise from the nanoscale, cellular morphologies of the residual tantalum layers and from their reduced electrical thicknesses. The transport in the nanostructured tantalum films is in the diffusive regime, and the conductivity becomes limited by roughness of the boundaries at the tantalum/tantala interfaces, at the tantalum/silicon-dioxide interface, and at the tantalum/alumina interface. Within each curve in the graphs of Fig. 7, the rise in the thickness-dependent resistance is mainly due to narrowing the conducting intervals between the oxide hillocks and opening additional channels for scattering. The relatively lower R_S values for the films formed at the lower anode potentials (see Fig. 7) can be explained by decreasing the amount of consumed tantalum in the film composition, as revealed by the TEM observations. In the case of reanodizing (Fig. 8), although N_h and N_w do not change with increasing E_R, the narrowing and thinning of all the four boundaries, accompanying by the expanding of the oxide hillocks, lead to further reduction of the mean free pass and to an increased contribution of the three-dimensional electron scattering within the nanowires in the directions normal to, and along, the substrate [17].

The fact that the films may have the extraordinary high resistance together with low TCR can be explained by considering the films as periodical heterogeneous multiphase (metal-insulator) systems, comprising an electron-conductive matrix with regularly distributed substoichiometric oxide having compositional depth and width profiles [18]. The negative TCR's and their increase with reducing the hillock sizes are a signature of the increased transition to hopping or tunneling conduction at elevated temperature, directly through the potential barriers, such as the hillock bases, or by means of electron traps in the tantalum monoxide percolating through the tantalum underlayer [19]. Further, as the hillock bases are mainly composed of oxygen-deficient TaO, they may behave as an acceptor semiconductor, which lowers the

temperature-dependent resistance [20]. Reanodizing of the films further thins and narrows the nanowires, while expanding the hillocks and increasing the potential barrier. This obstructs the electron tunneling and enhances the scattering, thus increasing the resistance and lowering the temperature coefficient of the films.

The simple explanation of the oscillatory character of the resistance vs potential curve (Fig. 9) can be the manifestation of QSE's [21]. As the nanostructured tantalum film is sandwiched between the two insulators—SiO_2 and Al_2O_3, the system can be treated as a symmetric quantum well (QW) or as an arrangement of very short quantum wires. The unconventional conductance properties revealed in the films may be due to contribution of ballistic transport phenomena that may occur when electrons travel across the nanowires whose length becomes shorter or at least comparable with the electron mean free pass [1, 19, 22, 23]. A number of authors have indicated the significant role played by the surface-roughness scattering in QW's, For example, scattering-induced level broadening suppresses QSE oscillations, and can lead to deviations from the $\lambda_F/2$ period, and even to a metal-insulator transition with decreasing film thickness [19, 24]. In the present case, the behavior of the R_S-E_R curve may, to some extent, result from the competition between the increment in the consumed tantalum and the roughness variation attributed to the localized oxide growth. Thus, due to the contrary contributions of these two factors, the QSE oscillations may diminish and, hence, may not be clearly seen on, or completely disappear from, some parts of the R_S-E_R curve. On the other hand, the fact that the QSE is already manifested at room temperature indicates a rather high degree of structural order in the films. Alternatively, it might results from possible effects due to other factors [21]. A detailed study of the oscillatory behavior of the anodized Ta-Al bilayers is expected in future works.

5. Summary and conclusions

(1) The Ta-Al metal bilayers, with various tantalum thicknesses, deposited onto oxidized silicon wafers were anodized in oxalic acid electrolytes at 21.5 to 53 V and then reanodized to relatively higher potentials, up to 80 V. The films formed under the porous alumina layers are composed of multiplied oxide nanohillocks separated from each other by unanodized tantalum metal, which is self-organized in the continuous network of tantalum nanowires, of possible width 25–10 nm, length 70–35 nm, and population density 10^9–10^{11} cm^{-2}, systematically depending on the initial tantalum thickness and the formation potential.

(2) The nanohillocks are composed of tantalum pentoxide mixed with substoichiometric tantalum oxides in the hillock depth. The innermost hillock parts, percolating through the residual tantalum film, are mainly oxygen-deficient tantalum monoxide.

(3) The mesh-like, nano-sized structure of the residual tantalum layers results in the extraordinary high sheet resistances (10^2–10^7 Ω/sq), owing to the enhanced three-dimensional electron scattering at the metal/oxide boundaries and at the wire interconnection points. Low negative TCR's, down to 5 ppm/K, are possible in the films formed at anode potentials higher 53 V.

(4) Oscillations of the potential-dependent resistance in the range 1–10 MΩ/sq at room temperature are due to quantum-size effects, consisted with the appearance of ballistic transport phenomenon in the films, which can be treated as an ordered arrangement of very short quantum wires sandwiched between the SiO_2 substrate and the overlying alumina layer.

(5) From a practical viewpoint, a significant feature is that two important parameters—high R_S and low TCR can be achieved in the same metal/oxide film. The approach to preparation of such films is of practical interest as it introduces technically simple, reproducible, and cost-effective way to fabricate self-planarized, integral and microchip resistors. The resistors thus formed will have high resistance together with excellent resistance thermostability. The films and fabrication processes developed here are fully compatible with the emerging semiconductor and hybrid-circuit technologies. This admits the integration of the resistors with the other electronic passives on a single chip module or microelectronic substrates [25]. On the other hand, it is of great interest to find applications of these self-assembled nanostructures that could benefit in unprecedented way from their unique and tunable properties in the field of nanoelectronics, optics, or biotechnology.

Acknowledgments

This work was supported in part by the Japan Society for the Promotion of Science through the award of a JSPS Invitation Fellowship for Research in Japan to A.M. The authors wish to thank ProfessorH.Habazaki of Hokkaido University (Japan) for his help with sputter-deposition of the Ta-Al bilayers onto oxide-coated aluminum foils. Thanks are due to Mr. A. Demianovich of Belmicrosystems R&D Co. (Belarus) for technical assistance.

References

1. B. BHUSHAN (Ed.), "Springer Handbook of Nanotechnology" (Spinger-Verlag, Berlin, Heidelberg, New York, 2003).
2. A. MOZALEV, M. SAKAIRI and H. TAKAHASHI, *J. Electrochem. Soc.* **151** (2004) F257–F268.
3. A. MOZALEV, M. SAKAIRI, I. SAEKI and H. TAKAHASHI, *Electrochim. Acta* **48** (2003) 3155.
4. A. MOZALEV, A. SURGANOV and S. MAGAINO, *ibid.* **44** (1999) 3891.
5. G. C. SCHWARTZ and V. PLATTER, *J. Electrochem. Soc.* **122** (1975) 1508.
6. *Idem., ibid.* **123** (1976) 34.
7. V. SURGANOV and A. MOZALEV, *Microelectron. Eng.* **37/38** (1997) 329.
8. S. LAZAROUK, S. KATSOUBA, A. LESHOK, A. DEMIANOVICH, V. STANOVSKI, S. VOITECH, V. VYSOTSKI and V. PONOMAR, *ibid.* **50** (2000) 321.
9. I. VRUBLEVSKY, V. PARKOUN, V. SOKOL and J. SCHRECKENBACH, *Appl. Sur. Sci.* **236** (2004) 270.
10. G. C. WOOD, in "Oxides and Oxide Films", edited by J. W. Diggle (Marcell Dekker, New York, 1987) Vol. 2, p. 41.
11. R. C. FURNEAUX G. E. THOMPSON and G. C. WOOD, *Corros. Sci.* **18** (1978) 853.
12. M. NAGAYAMA, H. TAKAHASHI and K. FUJIMOTO, in "Application of Complex Plane Analysis to Electrochemistry",

(USA Office of The Electrochemical Society of Japan, Cleveland, OH 1982) p. 1.
13. A. LLOYD SPETZ, D. SCHMEIBER, A. BARANZAHI, B. WALIVAARA, W. GOPEL and I. LUNDSTROM, *Thin Solid Films* **299** (1997) 183.
14. A. MOZALEV, Ph.D. thesis, Belarusian State University of Informatics and Radio-electronics, Minsk, 1992.
15. H. HABAZAKI, P. SKELDON, G. E. THOMPSON and G. C. WOOD, *Phil. Mag.* **B71** (1995) 81.
16. J. DE LAET, H. TERRYN and J. VEREECKEN, *Electrochimica Acta* **41** (1995) 1155.
17. F. J. HIMPSEL, J. E. ORTEGA, G. J. MANKEY and R. F. WILLIS, *Adv. Phys.* **47** (1998) 511.
18. L. MAISSEL and R. GLANG, "Handbook of Thin Film Technology" (McGraw-Hill, New York, 1970) Vol. 2.
19. M. MILUN, *Croatica Chemica Acta* **74**(4) (2001) 887.
20. K. CHU, J. P. CHANG, M. L. STEIGERWALD, R. M. FLEMING, R. L. OPILA, D. V. LANG, R. B. VAN DOVER and C. D. W. JONES, *J. Appl. Phys.* **91** (2002) 308.
21. E. I. ROGACHEVA, T. V. TAVRINA, O. N. NASHCHEKINA, S. N. GRIGOROV, K. A. NASEDKIN, M. S. DRESSELHAUS and S. B. CRONIN, *Appl. Phys. Lett.* **15** (2002) 2690.
22. D. A. WHARAM, T. J. THORNTON, R. NEWBURY, M. PEPPER, H. AHMED, J. E. F. FROST, D. G. HASKO, D. C. PEACOCK, D. A. RITCHIE and G. A. C. JONES, *J. Phys. C: Solid State Phys.* **21** (1988) L209.
23. C. J. MULLER, J. M. KRANS, T. N. TODOROV and M. A. REED, *Phys. Rev.* B **53** (1996) 1022.
24. M. JALOCHOWSKI, E. BAUER, H. KNOPPE and G. LILIENKAMP, *ibid.* **45** (1992) 13607.
25. A. MOZALEV, M. SAKAIRI and H. TAKAHASHI, in Proceedings of the 18th National Conference of Japan's Anodizing Research Society (ARS), 2001, Osaka, Japan, p. 55.

Received 12 January
and accepted 19 April 2005